Preferential Solvation in the Collisional Deactivation of Vibrationally Highly Excited Azulene in Supercritical Xenon/Ethane Mixtures

D. Schwarzer,* J. Troe, and M. Zerezke

Max-Planck-Institut für Biophysikalische Chemie, Am Fassberg, D-37077 Göttingen, Germany

Received: October 2, 1997; In Final Form: November 7, 1997

The collisional deactivation of vibrationally highly excited azulene was studied in equimolar supercritical mixtures of xenon and ethane at 385 K from gas- to liquid-phase densities. Azulene with an energy of ~20 000 cm^{-1} was generated by laser excitation into the S_1 state and subsequent internal conversion to the S_0* ground state. The loss of vibrational energy was monitored by transient absorption at the red edge of the $S_3 \leftarrow S_0$ absorption band at 290 nm. Transient signals were converted into energy−time profiles using hot band absorption coefficients from shock wave experiments for calibration and accounting for solvent shifts of the spectra. Under all conditions, the energy decays were exponential. At densities below 1 mol/L, the observed collisional deactivation rate constants k_c of the mixture were equal to the sum of the individual contributions of ethane and xenon collisions as expected from simple gas kinetics. At mixture densities above 2 mol/L, k_c is smaller than the deactivation rate constant found in neat ethane at half the density. This behavior can be rationalized by an isolated binary collision (IBC) model which relates the collision frequency Z to the radial distribution function $g(r)$ of an attractive hard-sphere particle in a Lennard-Jones fluid. Radial distribution functions obtained by Monte Carlo simulations clearly show that at high densities the less efficient collider xenon preferentially solvates the azulene molecule, reducing the number of azulene−ethane collisions and, therefore, the overall collisional deactivation rate constant with respect to neat ethane solutions.

I. Introduction

Collisional energy transfer of vibrationally highly excited molecules is a basic step of many kinetic phenomena in the gas and liquid phase. Indirect as well as direct techniques have been employed to determine its rate.[1,2] Among the detection techniques by which the stepwise energy loss could be monitored were UV absorption,[3−6] IR emission,[7,8] and energy-selective photoionization.[9]

The experimental results so far are best understood for isolated binary collisions in the gas phase. Although not all details have been clarified, much progress toward a quantitative description has been made in recent years.[11−14] The situation is much less satisfactory for the liquid phase. A series of experimental studies provided insight into the dynamics, while the quantitative analysis still appears fragmentary.[15−22] In particular, one may ask whether the dynamics of collisional energy transfer processes in dilute and in dense media are related at all. This question calls for experiments with the same excited molecule in environments of successively increased density. For a few systems such experiments are available now. Recently the collisional deactivation of azulene with an initial internal energy of 18 000 cm^{-1} was characterized quantitatively from the gas to the compressed liquid phase in a variety of supercritical solvents.[23] It was shown that the energy under all experimental conditions decays exponentially with time, leading to phenomenological deactivation rate constants k_c. For most of the collider gases, the density dependence of k_c is linear up to reduced densities of $\rho_r = \rho/\rho_c = 0.15$ where ρ_c is the critical density of the bath gas. At higher densities the further increase of the energy-transfer rate slows down and, finally, at $\rho_r > 1.5$ becomes faster again. These observations apparently are of general significance because studies with highly excited cycloheptatriene[24] led to quite similar results. The comparison of k_c with solvatochromic shifts $\Delta\nu$ of the azulene $S_3 \leftarrow S_0$ absorption band in ref 25 showed parallel density dependencies, which led to the conclusion that both quantities are determined by the same local density around the azulene molecule. By Monte Carlo simulations it was possible to represent this local density and to express k_c from the gas to the liquid phase in terms of an isolated binary collision (IBC) model in which average energies $\langle\Delta E\rangle$ transferred per collision are density-independent and collision frequencies Z are obtained from the radial distribution function $g(r)$ of an attractive hard-sphere (AHS) particle[26] in a Lennard-Jones fluid. Within this model, average energies $\langle\Delta E\rangle$ transferred per azulene−ethane collision were shown to be temperature- and pressure-independent in the range 298−640 K and 0.03−4000 bar, respectively.[25]

In the present article we further test this quantitative approach by experiments in bath fluid mixtures. These systems are characterized by differences in the $\langle\Delta E\rangle$ values and the local densities of the mixture components such that the influences of $\langle\Delta E\rangle$ and of local densities can easily be separated. This allows for a particularly sensitive test of the model. We report collisional energy transfer experiments of azulene in equimolar bath gas mixtures of xenon and ethane. First results have shown that at liquid densities k_c is smaller than the deactivation rate constant found in neat ethane at half the density.[27] As a result, we demonstrate that the AHS model excellently describes $k_c(\rho)$ of the mixture, with energy-transfer and interaction potential parameters determined earlier for the pure components. We, therefore, conclude that we now quantitatively understand collisional energy transfer of highly excited azulene from the dilute gas to the compressed liquid phase.

S1089-5639(97)03226-X CCC: $15.00
Published on Web 01/08/1998

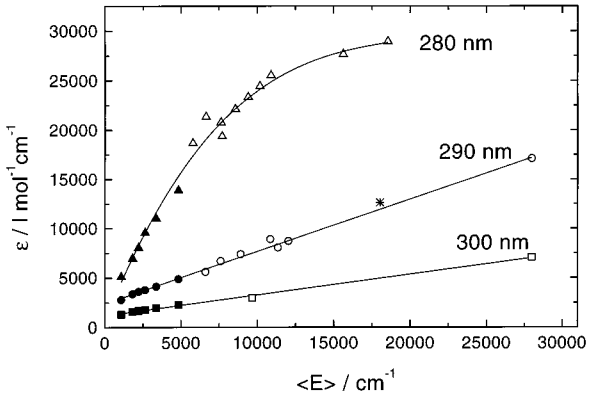

Figure 1. Energy dependence of azulene absorption coefficients in the gas phase at selected wavelengths (filled symbols, from static gas cell;[23] open symbols, from shock wave experiments;[29] (*) from laser excitation experiments[29]).

II. Experimental Technique

Azulene with a vibrational excess energy of 17 200−19 500 cm^{-1} was generated by laser excitation into the S_1 state followed by internal conversion to the electronic ground state within 1 ps.[28] The loss of vibrational energy was monitored at the red wing of the $S_3 \leftarrow S_0$ absorption band at 290 nm. In this article we present only a short survey of our experimental technique since the details have been reported before.[23,25,27] For low-pressure experiments, pulses from a frequency-doubled Nd:YAG laser at a wavelength of 532 nm were used for excitation. The 290-nm probe wavelength was obtained by second-harmonic generation of the output of a Rhodamine 6G dye laser operating at 580 nm which was pumped by a second frequency-doubled Nd:YAG laser. The delay between pump and probe pulses was adjusted electronically. The heatable sample cell with a path length of 20 cm was filled with 80−100 μbar of azulene and 30−100 mbar of collider gas. In these experiments only low time resolutions were required, being limited by the laser pulse width to 8 ns.

For experiments at high bath gas densities (>0.5 mol/L), pump and probe pulses were generated with a colliding pulse mode-locked (CPM) dye laser operating at a wavelength of 620 nm. After amplification the laser beam was focused in a 1 cm water cell generating a white light continuum. By means of an interference filter the desired probe wavelength of 580 nm was selected, amplified in two subsequent Rhodamine 6G dye cells, and frequency-doubled in a potassium dihydrogen phosphate (KDP) crystal generating the probe wavelength of 290 nm. Both laser pulses were fed into a standard pump and probe interferometer, recombined, and collinearly focused into the sample cell. The relative plane of polarization was adjusted to 54.7°. The width of the cross correlation of pump and probe laser pulses was 0.65 ps (fwhm), that is, sufficiently short to monitor all processes following the 1-ps preparation of vibrationally highly excited azulene. Experiments up to 1000 bar were performed in a heatable high-pressure cell with an optical path length of 2 cm.

The stepwise loss of vibrational energy of excited azulene as before was monitored by hot UV absorption spectroscopy near 290 nm. In this part of the azulene absorption spectrum, the energy dependence of the absorption coefficient ϵ is well-characterized (Figure 1), allowing the conversion of transient absorption signals into energy decay curves. For more details, see refs 23 and 25.

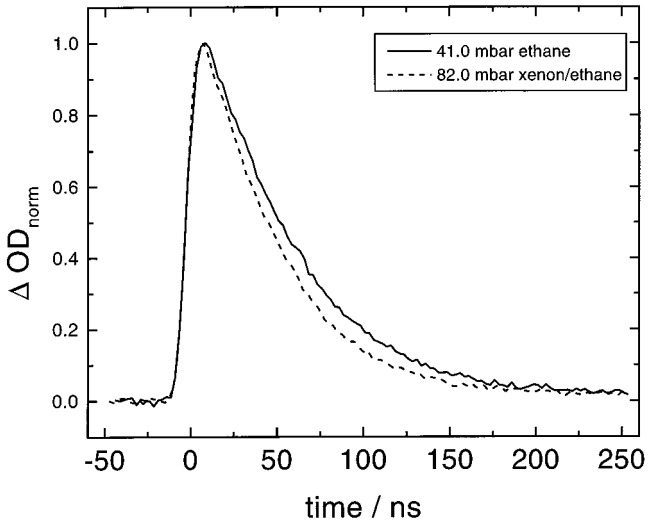

Figure 2. Comparison of absorption−time profiles recorded during the collisional deactivation of azulene at low densities and $T = 377$ K (full line, in 41 mbar ethane; dashed line: in 82 mbar equimolar mixture of xenon and ethane).

III. Results

In Figure 2 transient absorption signals recorded during the collisional deactivation of azulene in gas-phase ethane at 41 mbar and in a equimolar gas mixture of ethane and xenon at 82 mbar are compared. The temperature was 377 K. Both signals decay exponentially, and since the energy dependence of the azulene absorption coefficient ϵ at 290 nm is linear (see Figure 1), energy-loss profiles of the form

$$\langle E(t)\rangle = \langle E_0\rangle \exp(-k_c t) \tag{1}$$

were fitted to the data. $\langle E_0\rangle$ denotes the photon energy of the excitation pulse and k_c is a phenomenological deactivation rate constant. Considering that the slope of the energy decay curves gives direct access to average energies $\langle \Delta E\rangle$ transferred per collision[10] through

$$\mathrm{d}\langle E\rangle/\mathrm{d}t = Z\langle \Delta E\rangle \tag{2}$$

as long as the energy dependence of $\langle \Delta E\rangle$ is not too strong, and the distribution of excited molecules is sufficiently far from the final thermal equilibrium, an exponential energy decay leads to

$$\langle \Delta E\rangle = m_{\langle \Delta E\rangle}\langle E\rangle \tag{3}$$

with

$$m_{\langle \Delta E\rangle} = -k_c/\mathrm{Z} \tag{4}$$

being the slope of the linear $\langle \Delta E(E)\rangle$ curve. For dilute gas mixtures energy transfer is determined by collisions of azulene with individual components i:

$$\mathrm{d}\langle E\rangle/\mathrm{d}t = \sum_i Z_i\langle \Delta E\rangle_i \tag{5}$$

Considering eqs 1−4, the collisional deactivation rate constant for the mixture is

$$k_c = -\sum_i m_{\langle \Delta E\rangle_i} Z_i \tag{6}$$

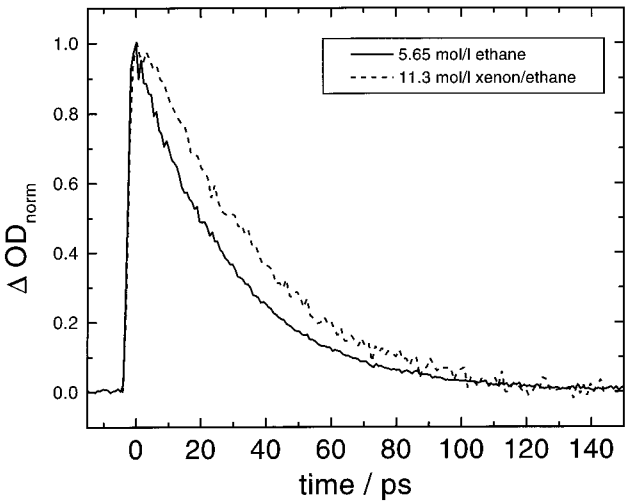

Figure 3. As Figure 2, at high densities and $T = 385$ K (full line: in 5.65 mol/L ethane; dashed line, in 11.3 mol/L equimolar mixture of xenon and ethane).

For collisions of azulene with xenon and ethane, $m_{\langle \Delta E \rangle}$ was determined to be -0.0073 and -0.0283, respectively,[25] when Z was identified with the Lennard-Jones collision frequency and Lennard-Jones parameters of $\sigma = 0.66$ nm and $\epsilon/k_B = 523$ K for azulene were used (values for ethane and xenon are tabulated in ref 30). From these values one expects an increase of k_c by 15% if to a given pressure of bath gas ethane the same partial pressure of xenon is added. This behavior is exactly observed in Figure 2: deactivation rate constants obtained from fitting eq 1 to the signals are 18.8 and 21.8 μs^{-1} for ethane and for the ethane/xenon mixture, respectively.

At high bath gas densities the situation changes markedly. The addition of xenon to ethane can lead to a decrease of k_c, as demonstrated in Figure 3. Here, signals obtained at densities of 5.65 mol/L of ethane and of 11.3 mol/L of ethane/xenon 1:1 mixture, respectively, are compared. It is striking to note that the energy decay slows down when xenon is added to a constant density of ethane in the fluid mixture. For a quantitative analysis of these signals, one has to consider that, at high densities, the azulene S_3 absorption band shifts to the red by $\Delta\lambda$ such that, with a constant probe wavelength of 290 nm, the energy decay is effectively monitored at a wavelength which in the gas phase would correspond to $\lambda_{eff} = 290$ nm - $\Delta\lambda$.[23,25] Since the energy dependence of the azulene absorption coefficient critically depends on the wavelength, see Figure 1, $\epsilon(\langle E \rangle)$ has to be evaluated at λ_{eff} by interpolation between 280- and 290-nm calibration curves. For xenon/ethane mixtures, $\Delta\lambda$ was determined from spectral shifts of azulene in neat solvents ethane and xenon such as characterized in ref 23 and 25. Assuming that eq 1 is valid also at higher densities and considering the finite time resolution due to the internal conversion process and the laser pulse cross correlation width of 0.65 ps, a model function (see eq 10 in ref 23) was evaluated and fitted to the data, yielding reliable values for k_c. In Figure 4 collisional deactivation rate constants of azulene in equimolar mixtures of xenon and ethane are plotted versus the ethane partial density and compared with k_c found in neat ethane at the same density.[23] For selected data pairs, the corresponding pressures are indicated as well. Densities of the mixture were determined with the method proposed by Pitzer[31] which is based on the theory of corresponding states. Pseudocritical constants of the mixture were derived from ref 32.

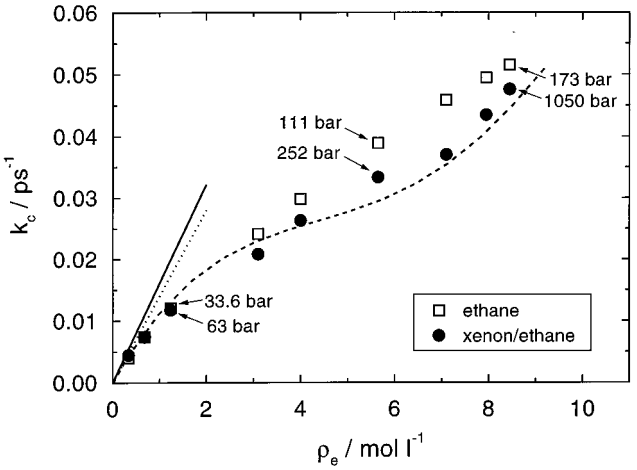

Figure 4. Density dependence of the collisional deactivation rate constant for azulene in 1:1 xenon/ethane mixture. k_c of the mixture (●) is plotted versus the ethane partial density and compared with the rate constant observed in neat ethane at that particular density (□) (full line, low-density limit for the mixture; dotted line: low-density limit for neat ethane; dashed line, simulation with the attractive hard-sphere collision model).

IV. Discussion

By comparing $k_c(\rho)$ with spectral shifts $\Delta\nu(\rho)$ of the azulene absorption spectrum, we have shown recently[25] that the density dependence of the collisional deactivation rate constant is determined exclusively by the local bath gas density in the immediate surrounding of the solute. This observation led to isolated binary collision (IBC) models (for an overview about IBC models see review 33) which relate the collision frequency Z to the radial distribution function around the considered molecule. Defining a collision as an event in which two molecules approach each other to within a certain distance, which for a hard-sphere solute of diameter σ_u in a hard-sphere solvent of diameter σ_v is given by $\sigma = (\sigma_u + \sigma_v)/2$, the collision frequency is expressed by[34,35]

$$Z^{HS} = Z_0 g(\rho,T,\sigma) \tag{7}$$

where $g(\rho,T,\sigma)$ is the value of the radial distribution function of the solute at contact with the solvent and Z_0 is the dilute gas collision frequency

$$Z_0 = \rho\sigma^2\sqrt{8\pi k_B T/\mu} \tag{8}$$

Delalande and Gale[26] added an attractive Lennard-Jones term to the solute−solvent hard-sphere potential to model relaxation rates of singly vibrationally excited small molecules in liquids. We applied this attractive hard-sphere (AHS) model successfully to explain the density dependence of collisional energy transfer rates of highly excited azulene in ethane.[25]

Assuming pairwise van der Waals interactions between solute and solvent, the density dependence of the spectral shift of the azulene absorption spectrum can be expressed in terms of radial distribution functions as well:[25]

$$\Delta\nu(\rho) \propto 4\pi\rho\int_0^\infty \frac{g(\rho,T,r)}{r^4}\mathrm{d}r \tag{9}$$

This relation was shown to be in excellent agreement with our $\Delta\nu(\rho)$ data of azulene in ethane if the same radial distribution functions were used as for modeling of the $k_c(\rho)$ data.[25]

In the following we will apply the AHS model to explain $k_c(\rho)$ in ethane/xenon mixtures considering eq 6 with hard-sphere collision frequencies from eqs 7 and 8 and keeping $\langle\Delta E\rangle$ values constant as in low-pressure gases:

$$k_c = -\sum_i m^{HS}_{\langle\Delta E\rangle i} Z^{HS}_i \tag{10}$$

$m^{HS}_{\langle\Delta E\rangle i}$ was evaluated by modeling the density dependencies of k_c in neat solvents xenon and ethane, respectively, in the framework of the AHS model. To determine $g(\rho,T,r)$, and consequently $g(\sigma)$ at the surface of the azulene molecule, the Monte Carlo method was used again.[36,37]

We treated solvent−solvent interactions by Lennard-Jones potentials,

$$V_v = 4\epsilon[(\sigma/r)^{12} - (\sigma/r)^6] \tag{11}$$

and azulene−solvent interactions by AHS potentials:[26]

$$V_u = \infty \quad r < \sigma$$

$$V_u = -\epsilon \quad \sigma \le r \le 2^{1/6}\sigma \tag{12}$$

$$V_u = 4\epsilon[(\sigma/r)^{12} - (\sigma/r)^6] \quad r > 2^{1/6}\sigma$$

At low densities, simulations were performed in a canonical ensemble of 107 solvent spheres (the binary mixture consisted of 53 particles of component 1 and 54 particles of component 2) and 1 solute sphere in a cubic simulation box with periodic boundary conditions. At high densities, up to 499 solvent spheres were used (the mixture then consisted of 249 particles of component 1 and 250 particles of component 2). The minimum image convention was used to calculate potential energies; interactions were truncated at half the box length. Starting from an initial face centered cubic structure, after equilibration up to 10^6 trials for each particle were taken to sample the configurational phase space. $g(r)$ around the solute was determined every five trials. Well depths for solvent−solvent interactions were $\epsilon_{ee}/k_B = 220$ K,[38] $\epsilon_{xx}/k_B = 230$ K,[39] and $\epsilon_{xe} = \sqrt{\epsilon_{ee}\epsilon_{xx}}$ (indices a, e, and x denote azulene, ethane, and xenon, respectively).

The adjustable parameters in these calculations ϵ_{ae} and ϵ_{ax} describing azulene−ethane and azulene−xenon interactions through eq 12, respectively, were obtained by modeling $k_c(\rho)$ and $\Delta\nu(\rho)$ data of azulene in neat solvents. Figure 5 shows corresponding results in xenon (from ref 23). As it turned out, the best agreement with the data is obtained with $\epsilon_{ax}/k_B = 900$ K. Results for $g(r)$ around the AHS particle azulene at 385 K and various densities are shown in Figure 6. For xenon a collision diameter of $\sigma_x = 0.38$ nm[39] was used. The solid line in Figure 6 is the low-density limit of $g(r)$, being the analytical solution of

$$g(r) = \exp\left(-\frac{V_u(r)}{k_B T}\right) \tag{13}$$

At $\rho = 0.48$ mol/L the radial distribution function from our Monte Carlo simulations is still close to this limit. However, around this density the peak at $\sigma_{ax} = (\sigma_a + \sigma_x)/2$ begins to decrease. The reason is that the number of xenon atoms in the immediate surrounding of the solute cannot increase linearly with the bulk density due to repulsive interactions. Simultaneously, a second peak around $(\sigma_{ax} + \sigma_x)$ grows in, reflecting the formation of a liquid structure. Around 18 mol/L the peak

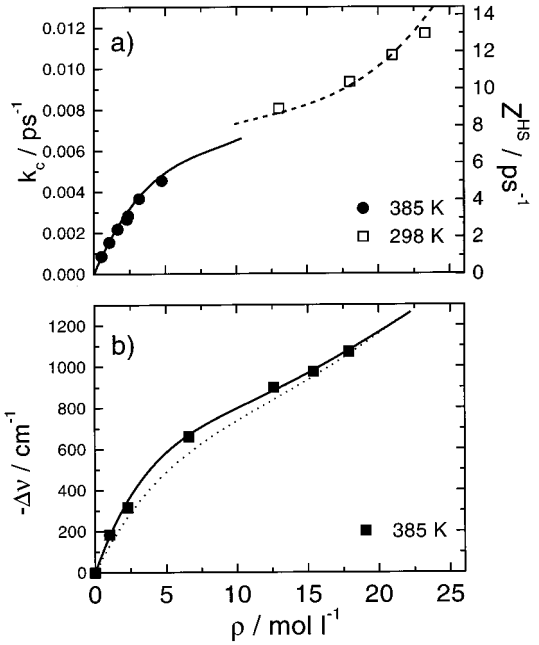

Figure 5. (a) Density dependence of collisional deactivation rate constants of azulene in xenon (full line, attractive hard sphere collision model at 385 K; dashed line, at 298 K). (b) Density dependence of shifts of the azulene $S_3 \leftarrow S_0$ absorption band in xenon (full line, simulation using relation 9 and $\epsilon_{ax}/k_B = 900$ K; dotted line, with $\epsilon_{ax}/k_B = 720$ K; see text).

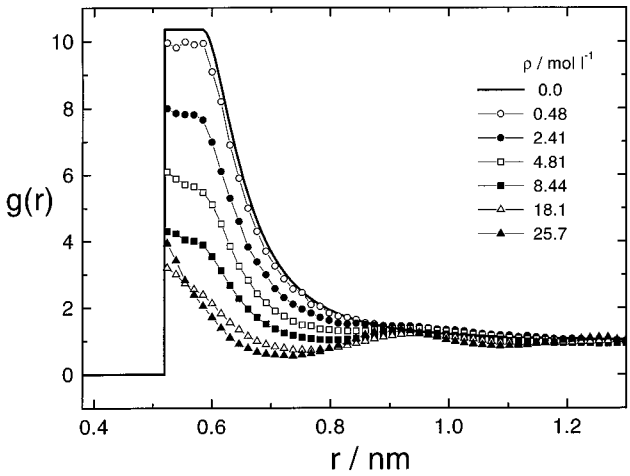

Figure 6. Radial distribution functions of an attractive hard-sphere particle in a Lennard-Jones fluid (xenon) at various densities ($\sigma_a = 0.66$ nm, $\sigma_x = 0.38$ nm, $\epsilon_{xx}/k_B = 230$ K, $\epsilon_{ax}/k_B = 900$ K, $T = 385$ K; see text).

at σ_{ax} reaches its minimum. At higher densities the peak increases again because the molecules in the first solvation shell are forced to stay at the surface of the solute due to repulsive interactions with the remaining solvent. This is the usual behavior in the compressed liquid and is independent of the attractive part of the potential.[40] Applying eqs 4, 7, and 8 by using $g(\sigma_{ax})$ values which were obtained from $g(r)$ curves by extrapolation, collisional deactivation rate constants were calculated via $k_c = m^{HS}_{\langle\Delta E\rangle} Z^{HS}$. Good agreement with the data points is obtained, when the slope of the $\langle\Delta E(E)\rangle$ curve in xenon is adjusted to $m^{HS}_{\langle\Delta E\rangle} = -9.0 \times 10^{-4}$, as demonstrated by solid and dashed lines in Figure 5a. $\Delta\nu(\rho)$ was modeled using the radial distribution functions of Figure 6 and relation 9. The agreement with the experiment again is very good, as shown by the full line in Figure 5b. The dotted line in Figure 5b is obtained if ϵ_{ax} is reduced by 20%. Similar calculations for the

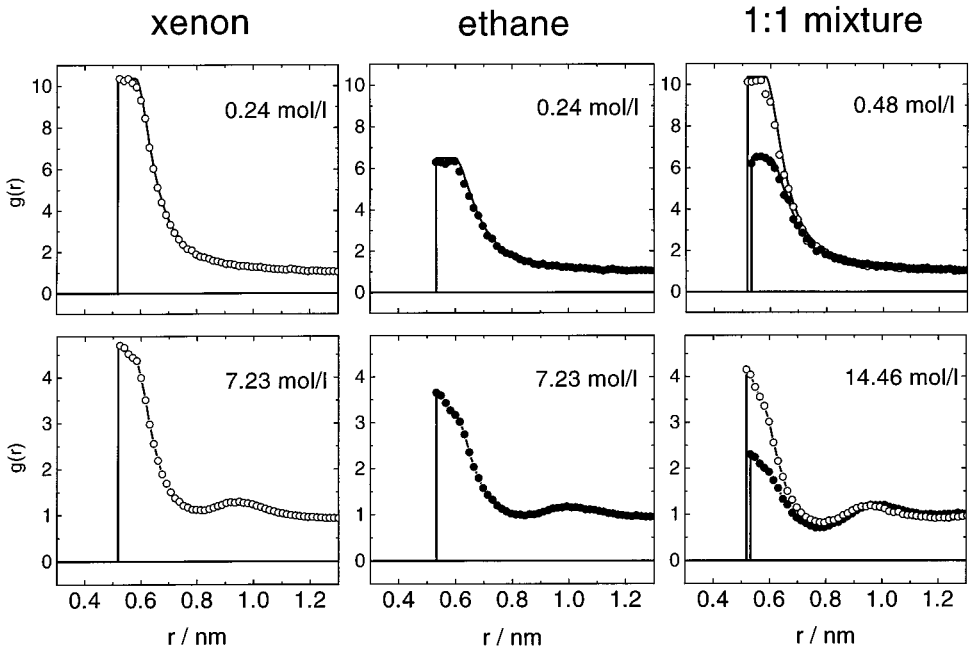

Figure 7. Comparison of radial distribution functions around an attractive hard-sphere particle in two different Lennard-Jones fluids (xenon and ethane) and their corresponding mixtures (upper half, at low densities; lower half, at high densities; $T = 385$ K; see text).

solvent ethane gave a value of $\epsilon_{ae}/k_B = 720$ K, as already demonstrated in ref 25. Using collision diameters of $\sigma_a = 0.66$ nm and $\sigma_e = 0.41$ nm[25] and expressing the hard-sphere collision frequency by eqs 7 and 8, one obtains $m^{HS}_{\langle\Delta E\rangle} = -5.5 \times 10^{-3}$ for the slope of the $\langle\Delta E(E)\rangle$ curve in ethane.

Considering that Lennard-Jones interaction parameters for azulene of 523 K $< \epsilon_{aa}/k_B <$ 590 K were estimated,[6,7] the well depths ϵ_{ax} and ϵ_{ae} obtained from our analysis seem to be very deep. However, the standard combining rule $\epsilon_{ij} = \sqrt{\epsilon_i \epsilon_j}$ is applicable only for nonpolar systems, and even there, pronounced deviations have been observed.[41] For polar (azulene)−nonpolar (xenon, ethane) interactions, the calculation of ϵ_{ij} is very complex and the standard combining rule is highly unreliable.[41] Therefore, well depths of $\epsilon_{ax}/k_B = 900$ K and $\epsilon_{ae}/k_B = 720$ K are feasible, in particular as these values are consistent with both, $k_c(\rho)$ and $\Delta\nu(\rho)$ (see Figure 5).

Having fixed all molecular and energy-transfer parameters for the individual bath gases, the next step in our analysis was to derive radial distribution functions from Monte Carlo simulations on an AHS particle in equimolar ethane/xenon mixtures and to calculate $k_c(\rho)$ on the basis of eq 10. Figure 7 compares corresponding results of $g(r)$ with those obtained in neat ethane and xenon at half the density. At partial densities of 0.24 mol/L (upper half of Figure 7) there is no difference between the Monte Carlo result of $g(r)$ and the analytical solution of eq 11, neither for the neat bath gases nor for the mixture. This indicates that under these conditions many-body effects can be neglected and both components of the mixture collide independently with the AHS particle. In this case the deactivation rate constant can be derived from eq 6 using a simple gas kinetic collision frequency. At high densities (partial densities of 7.23 mol/L, lower half of Figure 7) we observe a different behavior. Comparing with neat ethane, the addition of xenon reduces the value of $g(\sigma)$ for ethane from 3.7 to 2.3. At the same time $g(\sigma)$ for xenon only reduces from 4.7 to 4.2. Since ethane is a 6 times more efficient collider than xenon, k_c of the mixture is reduced. For these conditions, $k_c(\rho)$ of the mixture was calculated using eq 10 with hard-sphere collision frequencies from eqs 7 and 8 and energy transfer parameter $m^{HS}_{\langle\Delta E\rangle}$ evaluated above for the neat bath gases. The result, presented as a dashed line in Figure 4, is in excellent agreement with the experiment. One should emphasize that no adjustable parameter for the simulation of the mixture was used. We consider this result as strong support for our model. The energy transfer in a single binary collision event is a complex phenomenon whose modeling by classical trajectories is not simple but can be done.[14] However, once this part of the problem is solved, the density dependence of k_c can be characterized quantitatively by the calculation of the radial distribution function, for example, by Monte Carlo techniques such as described in ref 25 and in the present work.

V. Conclusions

The density dependence of the collisional deactivation rate constant k_c of highly excited azulene in binary mixtures of ethane and xenon was described in the framework of an IBC model which relates the collision frequency to the value of the radial distribution function $g(r)$ at the surface of the solute molecule and which assumes temperature- and density-independent average energies transferred per collision from the dilute gas to dense fluid phases. Having fixed all potential and energy-transfer parameters by modeling the density dependencies of k_c in neat xenon and ethane, respectively, the model successfully describes $k_c(\rho)$ of the mixture without any adjustable parameter. In particular the decrease of k_c at high densities, when xenon is added to ethane, is explicable through preferential solvation of azulene with the less efficient collider. In this way the present work provides a crucial test of the AHS model which appropriately accounts for local density effects on binary collision numbers.

Acknowledgment. Discussions of this work with J. Schroeder, K. Luther, and P. Vöhringer, as well as financial support by the Deutsche Forschungsgemeinschaft (Sonderforschungsbereich 357 "Molekulare Mechanismen Unimolekularer Prozesse"), are gratefully acknowledged.

References and Notes

(1) Quack, M.; Troe, J. *Gas Kinetics and Energy Transfer*; Ashmore, P. G., Donovan, R. J., Eds.; The Chemical Society: London, 1977; Vol. 2, p 175, Hippler, H.; Troe, J. In *Bimolecular Collisions*; Ashfold, M. N. R., Baggott, J. E., Eds.; Royal Society of Chemistry: London, 1989; p 209.

(2) Tardy, D. C.; Rabinovitch, B. S. *Chem. Rev.* **1977**, *77*, 396. Oref, I.; Tardy, D. C. *Chem. Rev.* **1990**, *90*, 1407.

(3) Hippler, H.; Troe, J.; Wendelken, H. J. *Chem. Phys. Lett.* **1981**, *84*, 257; *J. Chem. Phys.* **1983**, *78*, 6709.

(4) Hippler, H.; Luther, K.; Troe, J. *J. Chem. Phys.* **1983**, *78*, 6718. Damm, M.; H. Hippler, Troe, J. *J. Chem. Phys.* **1988**, *88*, 3564.

(5) Heymann, M.; Hippler, H.; Nahr, D.; Plach, H. J.; Troe, J. *J. Phys. Chem.* **1988**, *92*, 5507. Dove, J. E.; Hippler, H.; Plach, H. J.; Troe, J. *J. Chem. Phys.* **1984**, *81*, 1209.

(6) Hippler, H.; Otto, B.; Troe, J. *Ber. Bunsen-Ges. Phys. Chem.* **1989**, *93*, 428.

(7) Smith, G. P.; Barker, J. R. *Chem. Phys. Lett.* **1981**, *78*, 253. Shi, J.; Bernfeld, D.; Barker, J. R. *J. Chem. Phys.* **1988**, *88*, 6211. Shi, J.; Barker, J. R. *J. Chem. Phys.* **1988**, *88*, 6219.

(8) Toselli, B. M.; Brenner, J. D.; Yarram, M. L.; Chin, W. E.; King, K. D.; Barker, J. R. *J. Chem. Phys.* **1991**, *95*, 176.

(9) Hold, U.; Lenzer, T.; Luther, K.; Reihs, K.; Symonds, A. *Ber. Bunsen-Ges. Phys. Chem.* **1997**, *101*, 552.

(10) Troe, J. *J. Chem. Phys.* **1982**, *77*, 3485. Barker, J. R. *J. Phys. Chem.* **1984**, *88*, 11.

(11) Lim, K. F.; Gilbert, R. G. *J. Chem. Phys.* **1984**, *80*, 5501; **1986**, *84*, 6129.

(12) Stace, A. J.; Murrell, J. N. *J. Chem. Phys.* **1978**, *68*, 3028. Brown, N. J.; J. A. Miller, *J. Chem. Phys.* **1984**, *80*, 5568. Hippler, H.; Schranz, H. W.; Troe, J. *J. Phys. Chem.* **1986**, *40*, 6158.

(13) Bruehl, M.; Schatz, G. *J. Phys. Chem.* **1988**, *42*, 7223.

(14) Lenzer, Th.; Luther, K.; Troe, J.; Gilbert, R. G.; Lim, K. F. *J. Chem. Phys.* **1995**, *103*, 626.

(15) Wondrazek, F.; Seilmeier, A.; Kaiser, W. *Chem. Phys. Lett.* **1984**, *104*, 121.

(16) Seilmeier, A.; Scherer, P. O. J.; Kaiser, W. *Chem. Phys. Lett.* **1984**, *105*, 140.

(17) Sukowski, U.; Seilmeier, A.; Elsaesser, T.; Fischer, S. F. *J. Chem. Phys.* **1990**, *93*, 4094.

(18) Miyasaka, H.; Hagihara, M.; Okada, T.; Mataga, N. *Chem. Phys. Lett.* **1992**, *188*, 259.

(19) Schultz, K. E.; Russel, D. J.; Harris, C. B. *J. Chem. Phys.* **1992**, *97*, 5431.

(20) Sension, R. J.; Repinec, S. T.; Szarka, A. Z.; Hochstrasser, R. M. *J. Chem. Phys.* **1993**, *98*, 6291.

(21) Lenz, K.; Pfeiffer, M.; Lau, A.; Elsaesser, T. *Chem. Phys. Lett.* **1994**, *229*, 340. Elsaesser, T.; Kaiser, W. *Annu. Rev. Phys. Chem.* **1991**, *42*, 83.

(22) Hamm, P.; Ohline, S. M.; Zinth, W. *J. Chem. Phys.* **1997**, *106*, 519.

(23) Schwarzer, D.; Troe, J.; Votsmeier, M.; Zerezke, M. *J. Chem. Phys.* **1996**, *105*, 3121.

(24) Benzler, J.; Linkersdörfer, S.; Luther, K. *Ber. Bunsen-Ges. Phys. Chem.* **1996**, *100*, 1252.

(25) Schwarzer, D.; Troe, J.; Zerezke, M. *J. Chem. Phys.* **1997**, *107*, 8380.

(26) Delalande, C.; Gale, G. M. *J. Chem. Phys.* **1979**, *71*, 4804.

(27) Schwarzer, D.; Troe, J.; Votsmeier, M.; Zerezke, M. *Ber. Bunsen-Ges. Phys. Chem.* **1997**, *101*, 595.

(28) Schwarzer, D.; Troe, J.; Schroeder, J. *Ber. Bunsen-Ges. Phys. Chem.* **1991**, *95*, 933. Wagner, B. D.; Szymanski, M.; Steer, R. P. *J. Chem. Phys.* **1993**, *98*, 301.

(29) Brouwer, L.; Hippler, H.; Lindemann, L.; Troe, J. *J. Phys. Chem.* **1985**, *89*, 4608.

(30) Hippler, H.; Lindemann, L.; Troe, J. *J. Chem. Phys.* **1985**, *83*, 3906.

(31) Pitzer, K. S. *J. Am. Chem. Soc.* **1955**, *77*, 3427. Pitzer, K. S.; Lippmann, D. Z.; Curl, R. F., Jr.; Huggins, C. M.; Petersen, D. E. *J. Am. Chem. Soc.* **1955**, *77*, 3433.

(32) Prausnitz, J. M.; Gunn, R. D. *AIChE J.* **1958**, *4*, 430.

(33) Chesnoy, J.; Gale, G. M. *Ann. Phys. Fr.* **1984**, *9*, 893.

(34) Einwohner, T.; Alder, B. J. *J. Chem. Phys.* **1968**, *49*, 1458.

(35) Davis, P. K.; Oppenheim, I. *J. Chem. Phys.* **1972**, *57*, 505.

(36) Metropolis, N.; Rosenbluth, A. W.; Rosenbluth, M. N.; Teller, A. H.; Teller, E. *J. Chem. Phys.* **1953**, *21*, 1087.

(37) Allen, M. P.; Tildesley, D. J. *Computer Simulations of Liquids*; Oxford University Press: Oxford, 1987.

(38) Hirschfelder, J. O.; Curtiss, C. F.; Bird, R. B. *Molecular Theory of Gases and Liquids*; Wiley & Sons: New York, 1954.

(39) Kim, J. H.; Ree, T. *J. Chem. Phys.* **1989**, *91*, 3133.

(40) McQuarrie, D. A. *Statistical Mechanics*; Harper & Row Publishers: New York, 1973.

(41) Reid, R. C.; Prausnitz, J. M.; Sherwood, T. K. *The Properties of Gases and Liquids*, 3rd ed.; McGraw-Hill: New York, 1977.